Evaluation of the Maximum Cross-Correlation Method of Estimating Sea Surface Velocities from Sequential Satellite Images

ROBIN TOKMAKIAN

Institute of Oceanographic Sciences, Wormley, Godalming, Surrey, United Kingdom

P. TED STRUB

College of Oceanography, Oregon State University, Corvallis, Oregon

JULIE MCCLEAN-PADMAN

Department of Oceanography, Old Dominion University, Norfolk, Virginia

(Manuscript received 14 December 1989, in final form 29 June 1990)

ABSTRACT

We evaluate the method of estimating sea surface velocities from sequences of AVHRR and CZCS images using the maximum cross-correlation (MCC) technique. A set of synthetic images is created by advecting an AVHRR-SST field with a QG model velocity field. The MCC method of determining the sea surface velocities is then applied to the synthetic images. The rms differences and vector correlations between the model's velocity field and the field produced by the MCC method are presented. In addition, real AVHRR and CZCS images are used to find the rms difference between the satellite-derived velocity fields and in situ ADCP and hydrographic data. The tests show that AVHRR imagery yields the best results when images are separated by as short a period as possible. The rms errors at 6-h separation are on the order of 0.14 m s^{-1}, growing to $\geq$0.25 m s^{-1} at separations of more than 18 h. CZCS images are always separated by 24 h or more, but images with well-defined features may result in rms differences no larger than those produced by AVHRR images separated by 12 and 24 h. The method is most successful when several AVHRR image pairs separated by 12 h or less are available from a short (1–3 day) period and the velocity fields from the individual pairs are averaged to give a single synoptic picture of the current field. Specific examples show some of the reasons for incorrect vectors calculated by the method, and suggestions are made for improvements in the method.

1. Introduction

This study evaluates the maximum cross-correlation (MCC) method, objectively estimating sea surface velocities from sequences of satellite images. The method was originally developed for tracking clouds (Leese et al. 1971) and applied by Emery et al. (1986) to track oceanic features using sequences of infrared satellite images. Emery et al. compared the velocity field produced by the MCC method to surface drifter tracks and dynamic height fields and found qualitative agreement between the fields. Before the surface velocity fields calculated in this manner can be used in quantitative studies, the errors associated with the fields must be estimated. This is the goal of the present paper.

Some of the characteristics of the errors expected in velocity fields derived from sequential satellite images have been explored by Svejkovsky (1988) and Wahl and Simpson (1990). Svejkovsky used a subjective method of feature tracking, requiring an analyst to identify and track unique features from one image to the next. Using only the most identifiable features, Svejkovsky determined that subjective estimates of surface velocities differ from the velocities of surface drifters with an rms difference of 0.06 m s^{-1}. Svejkovsky used both Coastal Zone Color Scanner (CZCS) and Advanced Very High Resolution Radiometer (AVHRR) imagery to arrive at his conclusions. Wahl and Simpson used idealized models of uniform advection, horizontal diffusion, and surface heating to describe how the objective MCC method can be degraded by processes other than advection. The tests showed that nonadvective near-surface physical processes degrade the correlations between the image pairs over periods of less than 24 h. The greatest decrease in correlation was caused by spatially varying surface heating in the summer.

Two approaches are used to quantify the error in the sea surface velocity field estimated by the MCC method. In the first approach, a time series of synthetic

Corresponding author address: Dr. Ted Strub, College of Oceanography, Oregon State University, Oceanography Admin. Building 104, Corvallis, OR 97331-5503.

images is generated by advecting an initial AVHRR image with surface velocities from a high resolution quasi-geostrophic (QG) numerical model. The ability of the MCC method to recover the model velocities from the sequence of synthetic images is then quantified. In the second approach, velocity fields obtained from ship surveys are compared to the fields produced by applying the MCC method to nearly coincident CZCS and AVHRR images. Use of the synthetic images quantifies the error caused solely by rotation and distortion due to the geostrophic currents, without additional nonadvective processes. Use of the real sequences of images in comparison to field data quantifies the error caused by all sources. Comparison of the two approaches allows an estimate of the effect of nonuniform advection (rotation and distortion) and nonadvective processes (surface heating and mixing). One of the goals is to determine the relation between the temporal separation of the different types of images used in the MCC calculation and the rms error expected in the fields.

The differences between the AVHRR and CZCS images are: 1) what they see; 2) the depth to which they see into the water; and 3) the time separation between sequential images. The AVHRR sensor is an infrared instrument and thus sees the sea surface temperature (SST) in only the upper 15 μm of the ocean. In contrast, the visible channels used by the CZCS see differences in color caused mostly by phytoplankton pigment in the upper 5–15 m of the ocean. The CZCS sensor has the potential advantage of representing the upper ocean better than the AVHRR sensor. In practice, the SST seen by the AVHRR is found to be reasonably representative of the upper ocean when local winds blow between 5–10 m s^{-1}. Since neither temperature nor pigment concentrations are conservative in the upper ocean, it is best to keep the time separation between successive images short, in order to minimize the nonadvective processes. Here, the CZCS is at a disadvantage since it has a minimum separation of 24 h between images, while the minimum separation for the AVHRR images is 3–12 h depending on whether one or two satellites are operating. The differences between the two types of imagery provide the motivation to evaluate the rms errors of each.

2. Method and data description

a. MCC method

The MCC method has been described in detail by Emery et al. (1986), Garcia and Robinson (1989), and Wahl and Simpson (1990). A two dimensional space-lagged cross-correlation matrix (Press et al. 1986) is found for small regions in a pair of sequential images. The greatest positive correlation value is assumed to correspond to the location of the displacement of the first subimage in the second (larger) search subimage. The velocity vector at the center of the first subimage is calculated from this displacement and the time separation between the pair of images. The procedure is repeated for specified starting points over the image pair, either on a regular grid or at specific points for direct comparison to in situ data.

b. QG model and synthetic imagery description

To evaluate the velocity fields determined by the MCC method, a numerical model was used to produce synthetic SST fields. The Harvard Open Ocean Model (Robinson and Walstad 1987), a quasi-geostrophic model, was applied to an area off the northern California coast between 37°–40° N. Model resolution was 3 km with no bottom topography or surface forcing. CTD data from 18–26 May 1987, collected during the Coastal Transition Zone (CTZ) Experiment was used to initialize the model. The model velocity fields were used to advect an SST field from an AVHRR satellite image from 19 May 1987, producing synthetic images at regularly spaced times.

The advection equation is

$$\partial T/\partial t + u\frac{\partial T}{\partial x} + v\frac{\partial T}{\partial y} = 0, \qquad (1)$$

where T is the surface temperature and u, v are the velocity components provided by the model. A leapfrog time step and centered space derivatives were used, which introduced numerical dispersion, resulting in an artificial decrease in advective velocities (Mesinger and Arakawa 1976). For wavelengths longer than 11 km, attenuation of the true velocity is less than 10% (Tokmakian 1989). Since the subimage squares used in the MCC method have sides of 25–50 km, the numerical dispersion should not contribute significantly to errors in the displacements of these subimages, although it might distort the smaller features within the subimages reducing the correlations to some degree. The numerical dispersion is thus analogous to eddy diffusion in the real ocean, which is not included explicitly in the calculation of the synthetic images.

The domain of the model and synthetic images is limited to a region approximately 150 km × 340 km by the coverage of the hydrographic surveys used to initialize the model. Figure 1a shows this region, the locations where MCC velocities are calculated and the initial streamline field from the model. Velocities are to the southeast in the north of the domain and to the southwest in the southern half of the domain. Synthetic images for times 6, 12, 18, 24, and 30 h after the initial image were used in the analysis. Figures 1b–d show the synthetic images at 0, 12, and 24 h with lighter shades representing colder water. Advection of features to the southwest can be seen in the southern part of the sequence but the motion in the northern half is difficult to discern by eye.

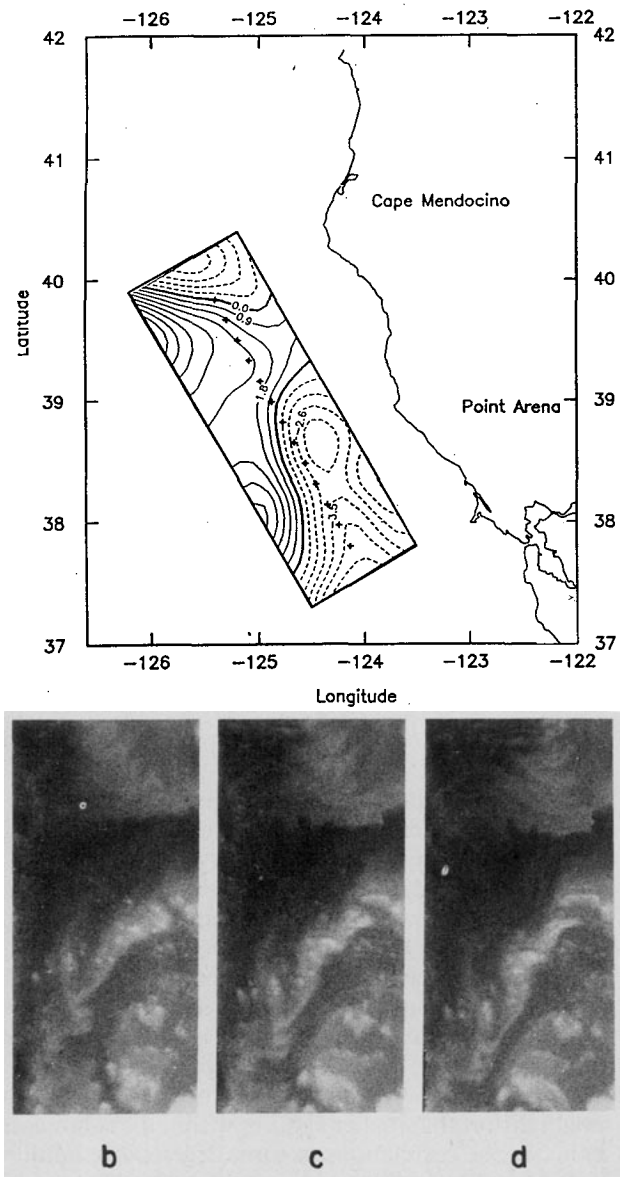

FIG. 1. (a) Streamlines of the QG model velocity field, showing the domain for the model and the synthetic images and the locations of the MCC grid points (crosses); (b) Synthetic SST field at 0 h (original AVHRR field); (c) at 12 h and (d) at 24 h:

c. *CODE and CTZ data description*

The satellite and field data available for comparison come from two experiments. The Coastal Ocean Dynamics Experiment (CODE) was located off northern California between approximately 37° and 39°N, extending offshore to about 125.5°W. The field data being used to evaluate the surface velocity field found by the MCC method is from the seventh leg of CODE-1, 4–10 July 1981 (Olivera et al. 1982). Two datasets are used for the comparison, the hydrographic dataset from which the dynamic heights (referenced to 500 db) and geostrophic velocities have been computed, and the acoustic Doppler current profiler (ADCP) dataset. Two sequential CZCS and four sequential AVHRR images were available from a cloud-free period 7–8 July 1981. The CZCS images occur at 1900 UTC with a separation of 24 h. The AVHRR images occur at 0300 and 1500 UTC, providing 12 (and 24) h separation times. The resolution of both sensors is approximately one kilometer. A 3 × 3 median filter was applied to the CZCS images to remove sensor noise (Denman and Abbot 1988).

The 1987 CTZ experiment was located off northern California between 39°–41°N. Field surveys from 18–26 May and 9–18 June provide fields of geostrophic velocities and dynamic heights relative to 500 db. The clearest AVHRR images come from the period between these surveys from 31 May–2 June 1987 (the CZCS sensor was no longer in operation at this time). ADCP data is available from a north–south transect from 3 June 1987, 30 hours after the last of the clear images, which provides the best comparison to the MCC velocities from the AVHRR images. This period between the two surveys is the same as that simulated by the QG model used to produce the synthetic images. Thus, although the lack of true synopticity makes the comparison more qualitative during the CTZ experiment, the comparison between the synthetic image results and the real image results is more direct at that time.

d. *SST gradient and high-pass filter calculation*

Tests of the method are made using raw SST fields from the images, horizontal gradients, and high-pass filtered SST fields. Gradients are formed with unweighted centered differences with spatial separations of four pixels (4.4 km) in each direction as used by Emery et al. (1986). The high-pass filter is accomplished in two steps; first, using a low-pass filter consisting of a centered 23 × 23 pixel average. The low-pass filtered image is then subtracted from the original image to produce the high-pass filtered image. The gradient images consist of very narrow lines which are found to decorrelate quickly in time. The high-pass filtered images retain more of the original structure of the SST field on scales of 25 km but eliminate larger-scale structure.

3. Results

a. *Evaluation using synthetic images and model velocities*

Initially the effect of different subimage sizes and the effect of using the high-pass filtered and gradients images rather than raw SST images was tested. The subimage size in the first image is varied from 25 to 50 km. The larger search areas in the second image are allowed to increase as the time separation between images increases, consistent with maximum velocities of

0.5 m s^{-1}. For separation periods of 30 h, this requires a search of 54 km in all directions covering the entire 150 km width of the synthetic image domain when the size of the initial subimage is added to the displacement. For this reason, 30 h is the maximum separation considered and the starting locations for the MCC calculation are limited to the 13 grid points along the center of the domain (Fig. 1a). Comparisons between the velocity fields are quantified in terms of the rms differences between the fields, calculated as:

rms difference

$$= \left\{ \left[\sum_i (u_{1i} - u_{2i})^2 + (v_{1i} - v_{2i})^2 \right] \Big/ N \right\}^{1/2} \quad (2)$$

where N is the number of vectors used in the rms difference formation and the subscripts 1 and 2 refer to MCC-derived and model (or measured) velocities, respectively.

The initial tests result in lower rms differences using the 50 × 50 km subimage size and raw SST rather than gradients. Use of the high-pass filtered images produces results similar to the raw SST images, except all cross correlations are lower in value. Subimages of approximately 25 × 25 km produce unacceptably high rms differences (greater than 0.38 m s^{-1}) for all but the shortest separation time (rms difference = 0.12 m s^{-1} at 6-h separation). When gradient images are used, the rms difference increases to 0.20 m s^{-1} for the 6-h separation, and to 0.59 m s^{-1} for longer separations. The maximum correlation values associated with each vector average about 0.78 for raw SST fields separated by 6 h, while application of the gradient operator and high-pass filter cause the average correlations to drop to approximately 0.4. Based on these tests, a 50 × 50 km subimage size is used in all analyses discussed below and the gradient operator is not applied. The high-pass filter is used with one pair of images from the 1987 period, but the results are the same as those obtained using raw SST images.

Figure 2a shows both the rms differences and the average of the vectors' associated maximum correlations as a function of the separation time in hours. As the separation increases, the average of the maximum correlation coefficients associated with the vectors decreases while the rms difference increases. Differences in rms increase from 0.14 to 0.22 m s^{-1} as the separation times increase from 6 h to 18 h. For separation times of 24 h and greater, the rms differences are approximately 0.4 m s^{-1}.

Figure 2b shows the same information as Fig. 2a for the average of velocity fields (from pairs of synthetic images separated by the same time period over 3–4 days) compared to the model velocity field. This averaging causes the rms difference to drop from 0.14 to 0.11 m s^{-1} for 6-h separation (seven image pairs), from 0.22 to 0.11 m s^{-1} for 12-h separation (six image pairs), and from 0.36 to 0.30 m s^{-1} for 24-h separation (four image pairs). The rms difference for the 18-h separation average stays about the same at 0.22 m s^{-1} (five image pairs).

Another measure of the similarity of the two velocity fields is provided by the complex correlation of the velocity vector field from the model with the field produced by the MCC method. The calculation of complex correlations, written in polar coordinates as $\rho = \rho_v e^{i\theta}$, is described in Kundu (1976) and Bendat and Piersol (1986). For the purposes of this paper, the magnitude of the complex correlation, ρ_v, is called the field correlation to distinguish it from the scalar correlation values (correlating SST subimages) associated with individual vectors computed with the MCC method. Figure 3a shows the field correlation as a function of the separation time found by correlating the model fields and the MCC fields. The dashed line shows the approximate 95% significance level for 13 random vectors as determined by a repeated "bootstrap" randomization of the original data. The field correlations are high and significant for separation times less than 24 h, but not for separations of 24 h and greater. These field correlation values are plotted against the corresponding rms differences in Fig. 3b, and show that high vector field correlation values are associated with low rms values.

Once the velocity vector field is produced by the MCC method, a vector consistency check (VCC) can be applied to improve the estimate of the displacements (Collins and Emery 1988). This check determines whether the displacement associated with each vector lies within ±1 standard deviation of the mean x and y displacements of its neighbors. If it does not, a new vector is found which has the maximum correlation in a region around the mean displacement of the neighbors. For the one-dimensional line of points used with the synthetic images, the four nearest neighbors (two above and two below) are used. For the two-dimensional fields used in comparison to the in situ data below, the eight nearest surrounding points (two points in each direction) are used. If a vector fails the consistency test, a region 20 pixels by 20 pixels, centered on the mean displacement of the neighbors, is searched for the maximum correlation to define a new displacement. For the synthetic images, the consistency check did not change the results for the image pairs separated by the shorter time periods (6–18 h). It did reduce the rms values for the images separated by 24 h from 0.36 to 0.23 m s^{-1}, and from 0.42 to 0.29 m s^{-1} for the images separated by 30 h.

b. Evaluation using real imagery and field data

The comparison of model velocities to MCC velocities derived from the synthetic images is a "best case" test. The synthetic fields are only affected by the small amount of numerical diffusion and the degree or rotation and distortion contained in the QG model, in

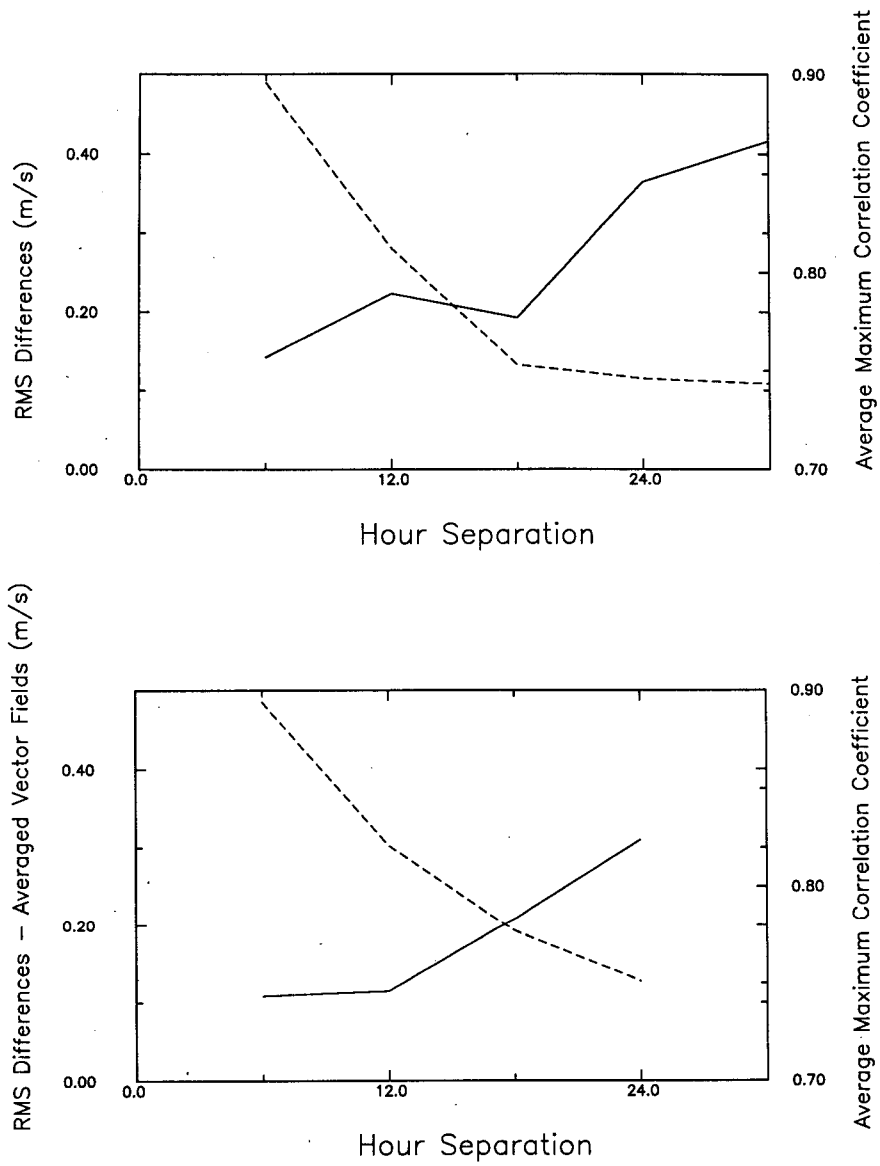

FIG. 2. (a) The effect of time separation on the rms difference (solid line) between model and MCC velocities and the average of the maximum cross-correlation values associated with the MCC vectors (dashed line); (b) As in Fig. 2a except using vector fields averaged over all pairs with the same time separations.

addition to the translation which the method attempts to retrieve. MCC velocities derived from real images are affected by additional nonadvective processes (surface heating, mixing, and ageostrophic motion), which cause the maximum correlations to be lower than those found from the synthetic images. To test whether the maximum correlation found for a given subimage region is greater than that expected for random correlations, an approximate 95 percent confidence limit is used. The value of this confidence limit is found by applying the MCC method to images separated by approximately one year, assuming all correlations between the images to be random. The 95 percentile value for all of the maximum correlations found between the images is used as the confidence limit. When raw SST images are used, the value is 0.80. When the high-pass filtered images are used the value is 0.40. Vectors associated with maximum correlations below this value are eliminated from the final velocity field. The final velocity fields produced with the high-pass filtered images and the lower 95 percent cutoff are similar to those produced with raw SST images and the higher cutoff. No further distinction between them are made.

Several AVHRR images are available from the same

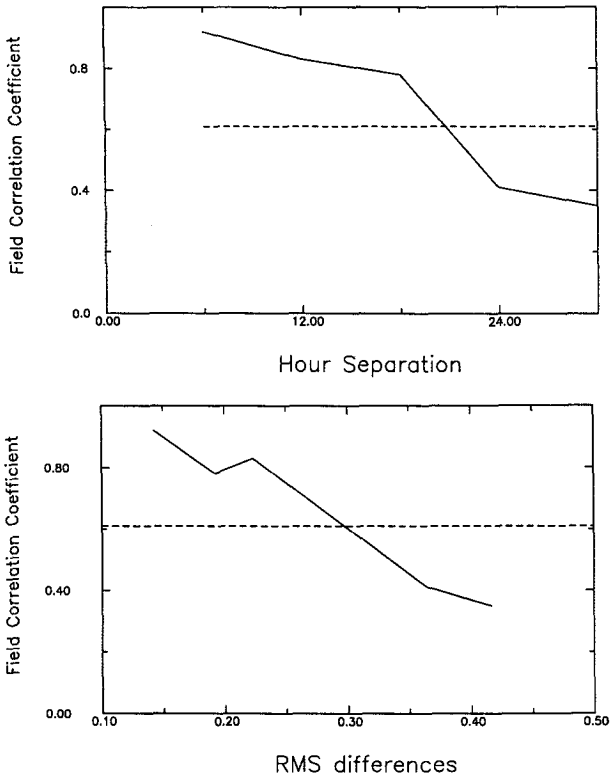

FIG. 3. (a) The effect of time separation on the magnitude of the complex correlation between MCC and model velocities (solid line). The dashed line shows an estimate of the 95 percent confidence limit. The magnitude of the complex correlation is called the field correlation, ρ_v; (b) The relation between the average vector field correlation, ρ_v, and the average associated rms difference, (m s^{-1}).

region and period as modeled to produce the synthetic images. Figure 4a shows the MCC velocities derived from a pair of high-pass images from 1–2 June 1987, separated by 14 h. The vectors are superimposed on the second high-pass filtered image of the pair. The velocity field shows the large-scale meander off Cape Mendocino and Point Arena, in general agreement with the southeastward flow south of Cape Mendocino and southwestward flow near Point Arena, seen in the streamlines derived from the 18–26 May 1987 cruise (Fig. 1a). The closest in situ data available for comparison come from a north–south ADCP transect from 3 June, approximately 30 h after the last image used in the MCC calculation. Figure 4b compares the ADCP and MCC velocities showing the general agreement in the change in direction from onshore to offshore flow at approximately 39.2°N. The rms difference between the ADCP and nearest MCC velocities (nine vectors) is approximately 0.15 m s^{-1}, similar to that obtained from the synthetic images under the same flow conditions. Figure 5 shows streamlines derived from the MCC field, in comparison to the dynamic height fields from surveys before and after the AVHRR image pair. Qualitative agreement with the meandering flow structure is good, although the difference in sampling times does not permit a more quantitative comparison.

The 1981 CODE dataset provides nearly coincident satellite and field (ADCP and geostrophic velocity) data which allows the best quantitative comparison of MCC and in situ velocity fields. In evaluating these comparisons, it is important to note that some of the variability comes from the sampling characteristics of the field data. In particular, the ADCP velocities are from a depth of 28 m while the MCC velocities are from the surface. Variability is also introduced by the time taken to complete the survey (approximately seven days), and by the interpolation of dynamic heights to a regular grid before calculation of geostrophic velocities. The variability in the field data can be quantified by finding the rms difference between the geostrophic and ADCP velocities, which is 0.25 m s^{-1}. This is probably a "worst case" comparison due to the very irregular sampling of the survey.

The gridded geostrophic velocity field (referenced to 500 db) is shown in Fig. 6a. Figure 6b shows the MCC velocity field from the CZCS image pair after eliminating vectors with associated correlation coefficients less than 0.8 and applying the vector consistency check. The rms difference between the geostrophic velocities and the MCC velocity field in Fig. 6b is 0.22 m s^{-1} and the field correlation is 0.58. Figure 6c shows the MCC velocity field derived from a pair of AVHRR images separated by 24 h on 7–8 July. The rms difference between the geostrophic velocities and this field is 0.22 m s^{-1} and the field correlation is 0.56. The best comparison is between the geostrophic velocities and the average of three MCC velocity fields derived from AVHRR images separated by 12 h shown in Fig. 6d. The rms difference is 0.18 m s^{-1} and the field correlation is 0.64. Statistics for all of the comparisons between geostrophic and MCC velocities are presented in Table 1. Application of the vector consistency check usually (not always) improves the comparison; averaging of several fields improves the comparison for the three AVHRR pairs separated by 12 h but not the two pairs separated by 24 h.

Figure 7a shows the velocity field at 28 m depth from the ADCP dataset. Figure 7b shows all the vectors derived from the CZCS image pair at the ADCP locations and Figs. 7c,d show the vectors derived from CZCS and AVHRR pairs of 7–8 July (24-h separation) after application of the consistency check and the correlation cutoff. Table 2 presents statistics comparing the ADCP velocities to the MCC velocities computed at the ADCP locations. Rms differences are approximately 0.3 m s^{-1}, larger than those comparing geostrophic and MCC velocities (Table 1). Applying the consistency check reduces the rms difference and increases the field correlation of the individual fields. Averaging the AVHRR fields does not improve the statistics of the 24-h fields, although it does reduce the rms differences for the 12-h fields (last two lines in

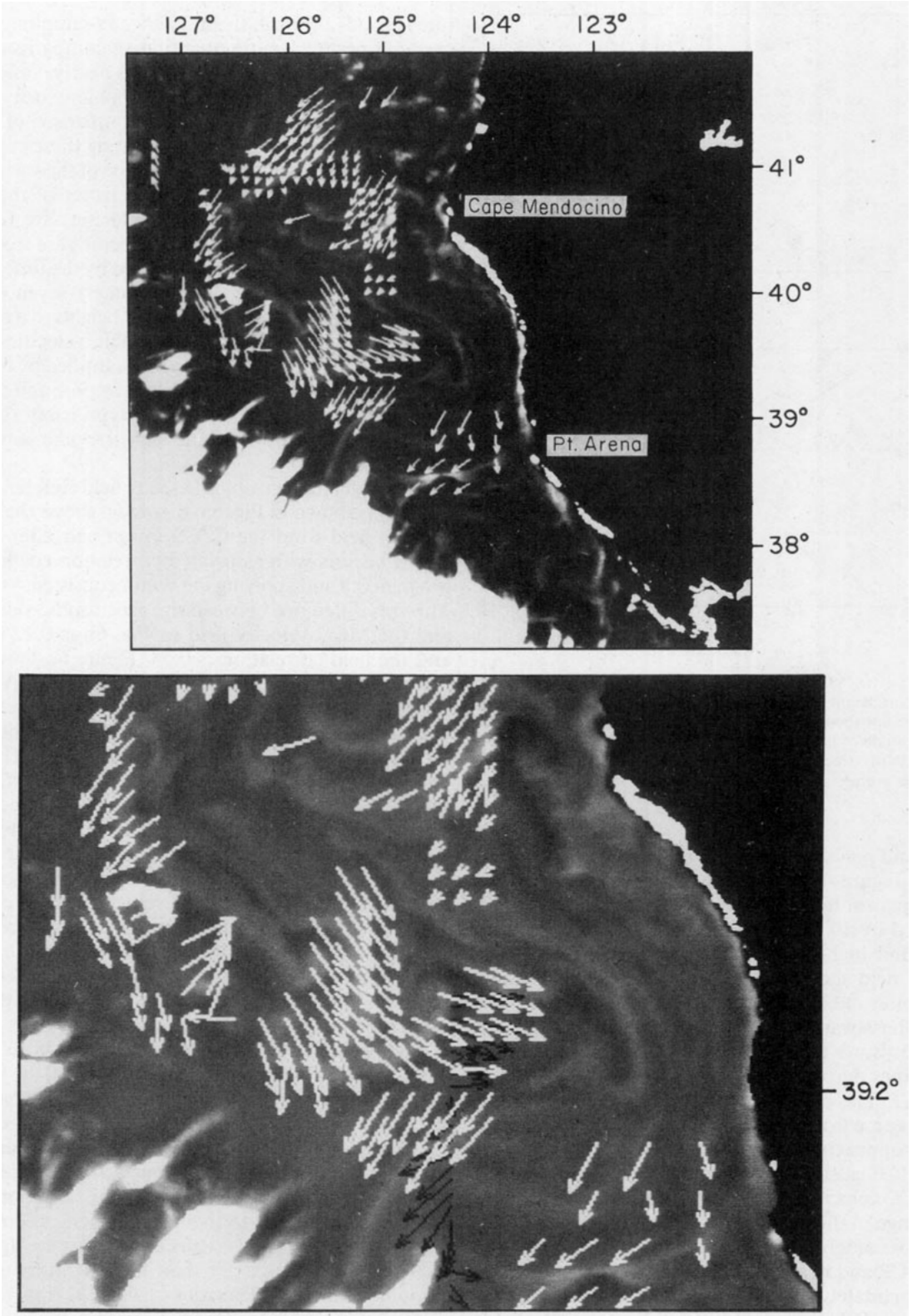

FIG. 4. (a) The displacement field obtained by applying the MCC technique to high-pass filtered AVHRR images collected at 2200 UTC 1 June and 1200 UTC 2 June 1987, overlaid on the high-pass filtered 2 June image; (b) An expanded view of Fig. 4a, showing ADCP velocities (black vectors) in comparison to the MCC velocities (white vectors).

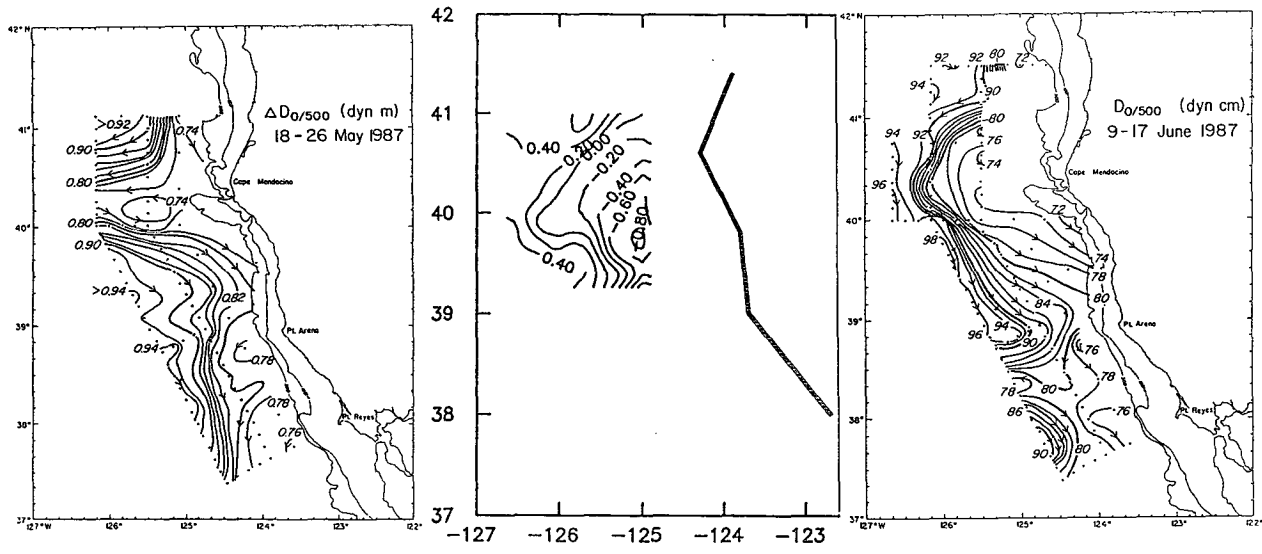

FIG. 5. Dynamic height fields from surveys on 16–26 May 1987 and 9–17 June 1987 in comparison to streamlines (center) derived from the MCC vectors shown in Fig. 4a.

Table 2). Field correlations are slightly higher for the CZCS-derived vectors in comparison to ADCP velocities than they were in comparison to geostrophic velocities. Field correlations are generally lower for the AVHRR-derived vectors, although the maximum value found for one AVHRR pair is higher ($\rho_v = 0.61$ for day 188/189–12 h, after the VCC check is applied).

Examining Figs. 6, 7 qualitatively shows that the MCC method resolves the westward flow at approximately 38.5°N, 124°–125°W. The averaged 12-h AVHRR velocity field (Fig. 6d) resolves the southeastward flow at 37.5°N, 124°–125°W better than the velocity field from the CZCS image pair (Fig. 6b). The southward flow from 38.5°N down to 38°N, 124°W is also resolved by the averaged field. In general, there are more significant vectors produced by the AVHRR images than by the CZCS images. The ADCP velocities are greater than the MCC and geostrophic velocities, there is also more small-scale structure in the ADCP velocities (Fig. 7a) than in the geostrophic velocities (Fig. 6a). Use of the 50 km subimage in the MCC calculation picks out only the large-scale flow structure and the MCC fields are more like the smoother geostrophic velocity field than the ADCP field, as reflected in the higher rms differences with the ADCP field.

4. Discussion

Physical and biological processes not included in the MCC method account for much of the difference between the MCC fields and either the model velocity fields or the in situ data. For the AVHRR images, these processes can be discussed by examining a simplified equation for the conservation of heat at the surface of the ocean:

$$\partial T/\partial t + \mathbf{V}_h \cdot \nabla_h T = S + K_h \nabla_h^2 T + K_z \frac{\partial^2 T}{\partial z^2} - w \frac{\partial T}{\partial z} \quad (3)$$

where the horizontal and vertical velocities have been shown separately, as have the horizontal and vertical eddy diffusivities (K_h, K_z), and S is the total surface heating by sensible, latent, and radiative heat flux. An equivalent equation can be formed for chlorophyll concentrations by replacing heating sources and sinks by biological sources and sinks. The MCC method assumes only horizontal translation of features in $\mathbf{V}_h$. Tests with the QG model quantify the error due to rotation and distortion caused purely by the large-scale geostrophic component of $\mathbf{V}_h$. Rotation and distortion caused by the ageostrophic part of $\mathbf{V}_h$ affect the real images but not the synthetic images. Other physical factors which affect the real images are represented by the terms on the right side of Eq. (3). These include vertical and horizontal mixing and advection. Surface heating and cooling affects the AVHRR images; biological growth, grazing, and sinking contribute to changes in the CZCS images.

Wahl and Simpson (1990) have used idealized models to estimate the effect of some of the processes on the right of Eq. (3). They find that horizontal diffusion has only a minor effect over time separations of 24 h and less, for values of K_h less than 100 $m^2 s^{-1}$. Spatially uniform surface heating and cooling has a greater effect, but is still only moderately important for time separations of 12 h and less. They find the most rapid decrease in correlation coefficients to be associated with spatially varying heating, caused by broken stratus clouds. This may limit the length of acceptable time separations between images to 6–9 h.

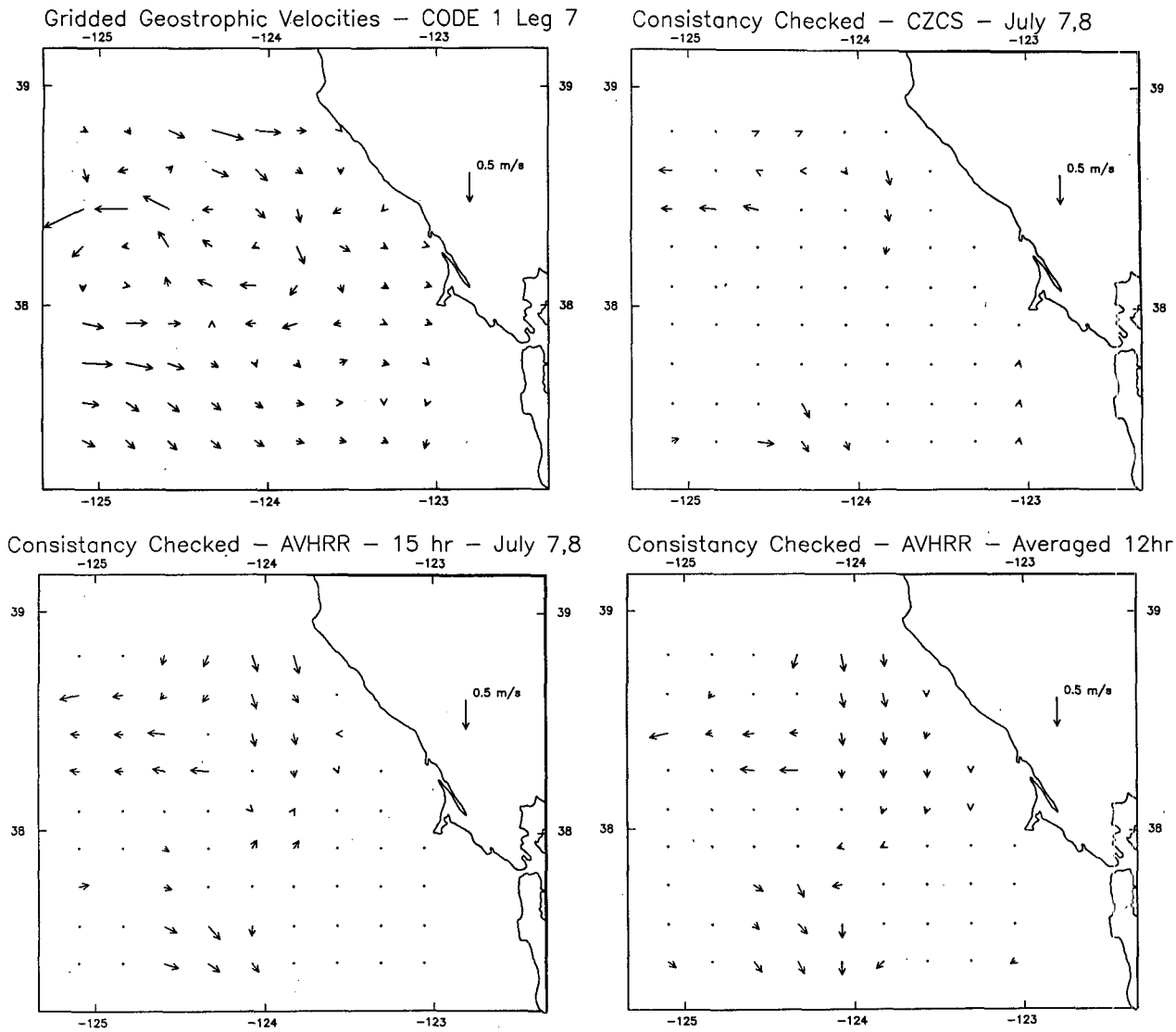

FIG. 6. (a) Velocity field from the gridded dynamic heights during CODE-1, 4–10 July, 1981; (b) Velocity field derived from CZCS images 7–8 July 1981 (24-h separation) after a vector consistency check and significance cutoff are applied; (c) Velocity field derived from AVHRR images 7–8 July 1981 (24-h separation) after a vector consistency check and significance cutoff are applied; (d) Average velocity field derived from 3 AVHRR image pairs, 7–8 July 1981 (24-h separations) after a vector consistency check and significance cutoff are applied.

They did not evaluate the effect of vertical mixing. The present results place geostrophic rotation and distortion intermediate between spatially uniform and spatially variable surface heating, degrading the cross correlations at separation times of 12 h and more. This result may be somewhat site specific, reflecting the relatively energetic nature of the meanders and jets in the California Current.

These nonadvective processes reduce the correlation coefficient in the region corresponding to the correct displacement of water parcels and allow the MCC method to find spurious incorrect displacements. When all of the MCC vectors derived from an image pair are plotted, as in Fig. 7b, a number of such clearly incorrect vectors are evident. Most of these are eliminated from the final field because of their low maximum correlation coefficient, resulting in a sparse velocity field, as in Fig. 7c. Examination of the details of these spurious correlations provides some insight into the circumstances under which the MCC method fails.

The large velocities represented by the two vectors marked A and B in Fig. 7b are different from the ADCP velocities from these locations in Fig. 7a, which were surveyed on 7–8 July, close to the time of the images. Thus, these incorrect velocities do not come simply from a lack of synopticity. The MCC velocities at these points are also different from the neighboring MCC velocities. Examination of one of the CZCS images

TABLE 1. Comparison to dynamic heights.

Correlation pair	Time	rms	ρ_v	θ
Day 188/189 CZCS—19 h	24	0.24	*0.52	−10.7
Day 188/189 CZCS—VCC	24	0.22	0.58	−10.9
Day 188/189 AVHRR—15 h	24	0.22	0.48	−26.1
Day 188/189 AVHRR—VCC	24	0.22	0.56	−27.3
Day 188/189 AVHRR—03 h	24	0.25	*0.39	−47.5
Day 188/189 AVHRR—VCC	24	0.23	0.44	−43.3
Day 188 AVHRR—03, 15 h	12	0.26	0.55	−39.6
Day 188 AVHRR—VCC	12	0.23	0.59	−40.7
Day 188/189 AVHRR—15, 03 h	12	0.20	0.49	−19.0
Day 188/189 AVHRR—VCC	12	0.21	0.33	−10.7
Day 189 AVHRR—03, 15 h	12	0.23	0.51	−21.0
Day 189 AVHRR—VCC	12	0.21	0.55	−22.0
Average AVHRR—24 h VCC fields	24	0.24	0.47	−29.5
Average AVHRR—12 h VCC fields	12	0.18	0.64	−23.1

* Not significant, VCC = vector consistency check.

from the pair (Fig. 8a) shows that these ADCP data points (located approximately at 123.5°W and 38.3°N) are in regions with weaker gradients in pigment concentration, rather than near the sharp fronts in the CZCS images. The displacements with the highest correlations correspond to displacements to areas which are clearly incorrect, although the pattern of pigment concentrations of the area in the second image is similar enough to that in the first image to cause high correlations (note that the correlation calculation removes the mean of each subimage). The field of correlations associated with the vector labeled A in Fig. 7b is shown in Fig. 8b. There are two distinctly different areas with high correlation values, a more distant region to the northwest and a closer region to the south. A similar pattern exists for the point labeled B. Figure 8c shows an expanded view of the image, with arrows drawn from points A and B to both maxima. The correlation with the distant region is slightly higher but the measured velocity field in Fig. 7a shows that the secondary closer peak is really the correct displacement of the parcel of water.

This discussion brings out a disadvantage of the use of large search areas, which increases the chance of spurious large correlations. Since the size of the search window in the second image is determined by the maximum velocity and the time separation between images, this provides another reason to minimize the time between images, allowing smaller search windows to be used. Figure 8b also suggests that more intelligent search strategies might be adopted, which locate the maxima by following gradients and preferentially choosing closer maxima unless distant maxima are significantly greater and the more reasonable choice.

One reason for the slightly lower correlation of the closer point in Fig. 8b may be rotation of the feature. To test this, the initial subimage was rotated by increments of 5° before repeating the calculation of the correlation matrix. At −20°, the maximum correlation is found in the closer secondary maximum of the contour plot to the southeast. This test provides support for the conclusions of Vesecky et al. (1987) who state that rotations of greater than 15° reduce the ability of the MCC method to track features between images. It also suggests the need to efficiently include rotation in the MCC search, in agreement with Kamachi (1989) and Emery (pers. comm.).

To examine whether the rms differences in velocity discussed above are caused equally by errors in magnitude and direction, rms differences were formed separately for direction and magnitude, comparing MCC vectors to velocities from the model generated synthetic fields and the measured ADCP and geostrophic velocities. Figure 9a shows the rms difference in direction as a function of time separation for the synthetic images (dashed line). This difference increases slowly with time (dotted line) for separations of 6–18 h and more rapidly for longer separations. The rms differences in direction of the vectors between the in situ data and the MCC vector fields from 12 and 24 h separations are also shown (crosses) and are much higher. The greater errors found with the real data suggest that the processes other than geostrophic rotation and distortion (shown on the right side of Eq. 3) have a major affect on the satellite-derived surface circulation over time periods of 12 h and more, implying that real images should be separated by less than this, if possible.

The rms differences in magnitude are shown similarly in Fig. 9b. There is not a consistent distribution pattern in the rms magnitude differences, although the lowest values occur for separations of 6 h and the highest occur for 24 h. Results from the synthetic images suggest that distortion and rotation of the features causes errors in direction of less than 30° for separations of 6–18 h increasing to 60° at 24 hours. Since the vector error is a function of the cosine of the angle, rms errors of 13% and 50% are associated with angles of 30° and 60°. Comparison to in situ data suggests that by time separations of 12 h, errors of 50 percent are caused by errors in angle, corresponding to rms errors of 0.15 m s^{-1} for typical velocities of 0.3 m s^{-1}. Errors in the magnitude of the velocities range from 0.1 to 0.2 m s^{-1}. Thus, both types of errors contribute equally in real images separated by 12 h and more. The results from the synthetic images suggest that both can be reduced by using shorter time separations.

The rms differences found in this paper are much higher than the value of 0.06 m s^{-1} reported by Svejkosky (1988) who restricted the in situ surface drifter velocities used for comparison to be within five hours of the satellite image and further restricted the points to those that could be tracked easily by eye. As noted above, some of the rms difference is due to the variability in the field data and its sampling patterns, but much is also due to the MCC method itself, which has several disadvantages in comparison to the subjective method. Subjectively selecting features to track from one image to the next results in the use of the most

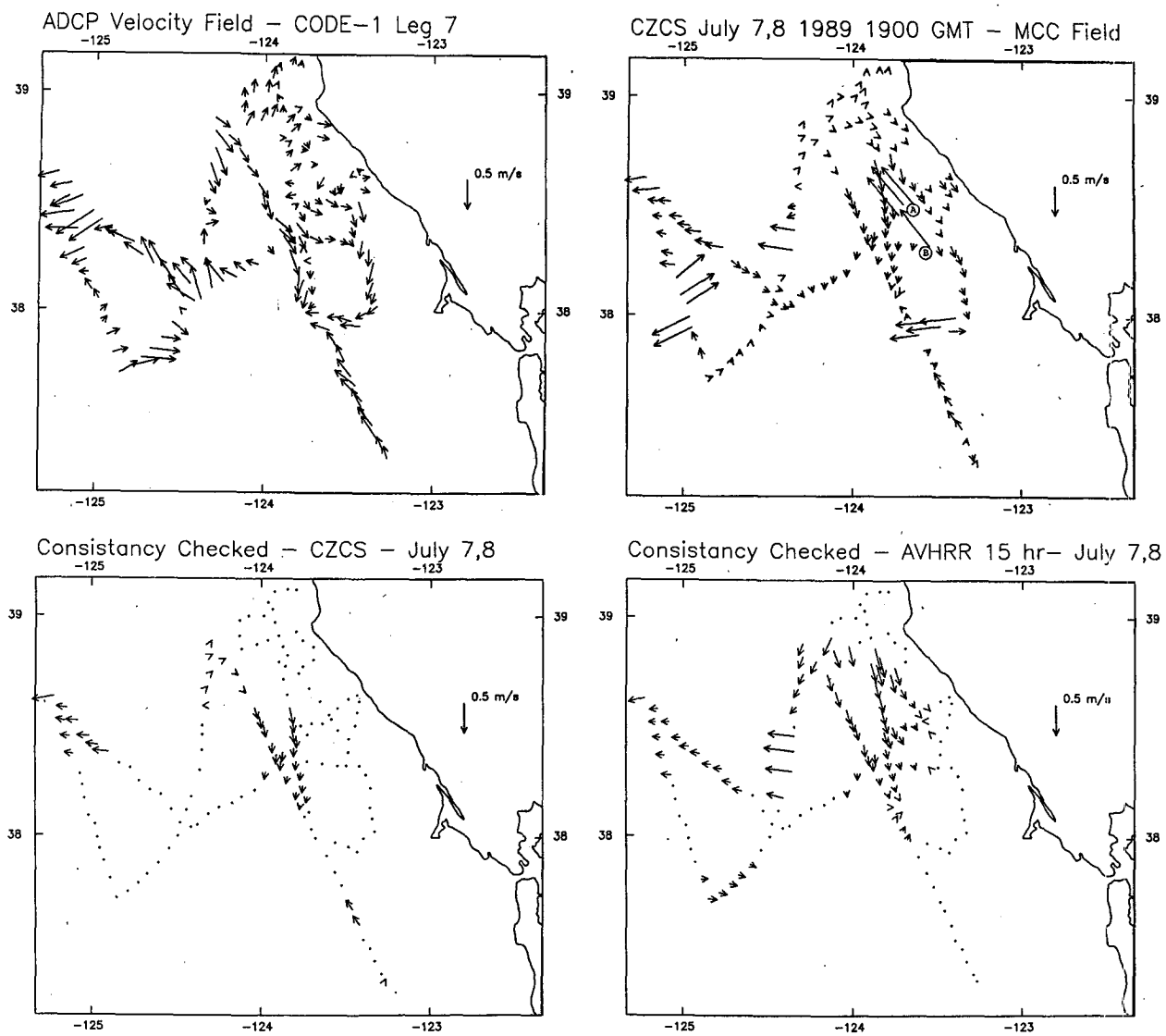

FIG. 7. (a) Velocity field from ADCP data during the same CODE-1 cruise as shown in Fig. 6a, 4–10 July 1981; (b) Complete velocity field derived from CZCS images 7–8 July 1981 (24-h separation). No significance cutoff or vector consistency check has been applied. Letters A and B denote starting locations for incorrect displacements discussed in section 4; (c) Velocity field derived from CZCS images 7–8 July 1981 (24-h separation) after the significance cutoff and vector consistency check are applied; (d) Velocity field derived from 2 AVHRR images 7–8 July 1981 (24-h separation) after the significance cutoff and vector consistency check and applied.

distinctive features, eliminating regions with low gradients. Rotation in features can also be followed more easily by eye. Visual inspection of the images results in an overall feeling for the pattern of changes in the image pairs, forcing the search to be restricted to only "reasonable" areas and reduces the chance of grossly incorrect displacements. The incorrect displacements shown in Fig. 7b would never have been found by visual tracking. In contrast to the subjective method, the objective MCC method, as used here, removes the guarantee that the feature being tracked is unique and easily identifiable. It allows searches of unreasonable areas which sometimes produce random, high correlations, and reduces the ability to follow rotating and distorting features. The lowest rms errors produced by the present MCC method applied to real images were obtained by averaging the three AVHRR fields with 12-h separation and was 0.18 m s^{-1}, three times the value found by Svejkosky. Tests with the synthetic images suggest that this might be reduced to around 0.10–0.15 m s^{-1} if images separated by 6 h were available.

It seems unlikely that the MCC method will ever yield rms errors as low as Svejkosky's 0.06 m s^{-1}. Even if this estimate is an overly optimistic assessment of the level of error that might be found for routine application of subjective feature tracking methods, the

TABLE 2. Comparison to ADCP.

Correlation pair	Time	rms	ρ_v	θ
Day 188/189 CZCS—19 h	24	0.27	0.64	−18.5
Day 188/189 CZCS—VCC	24	0.27	0.65	−19.7
Day 188/189 AVHRR—15 h	24	0.32	*0.18	−43.3
Day 188/189 AVHRR—VCC	24	0.28	0.38	−29.4
Day 188/189 AVHRR—03 h	24	0.31	*0.30	84.0
Day 188/189 AVHRR—VCC	24	0.24	*0.30	81.5
Day 188 AVHRR—03, 15 h	12	0.31	0.37	−42.2
Day 188 AVHRR—VCC	12	0.27	0.42	−42.8
Day 188/189 AVHRR—15, 03 h	12	0.27	0.49	−16.3
Day 188/189 AVHRR—VCC	12	0.23	0.61	−15.1
Day 189 AVHRR—03, 15 h	12	0.34	*0.29	−23.3
Day 189 AVHRR—VCC	12	0.29	0.37	−18.4
Average AVHRR—24 h VCC fields	24	0.28	*0.30	−67.7
Average AVHRR—12 h VCC fields	12	0.23	0.46	−29.7

* Not significant, VCC = vector consistency check.

discussion brings out a number of advantages of the subjective method. The advocates of objective methods emphasize the elimination of the human bias inherent in the subjective methods. This discussion makes it clear that the objective methods also eliminate the benefit of human insight, and substitute inferior computer-based pattern recognition for the more highly developed pattern recognition capabilities of human vision. The true advantages of the objective methods are: 1) the ability to automate and process large amounts of data; 2) uniform quality of the estimated fields; and 3) estimates of the uncertainties in the fields. The last point is important since fields of estimated uncertainties are necessary if the velocity fields are to be combined with other data in an optimal method. Based on the results presented here, an estimate of the spatially varying uncertainties in the surface velocities

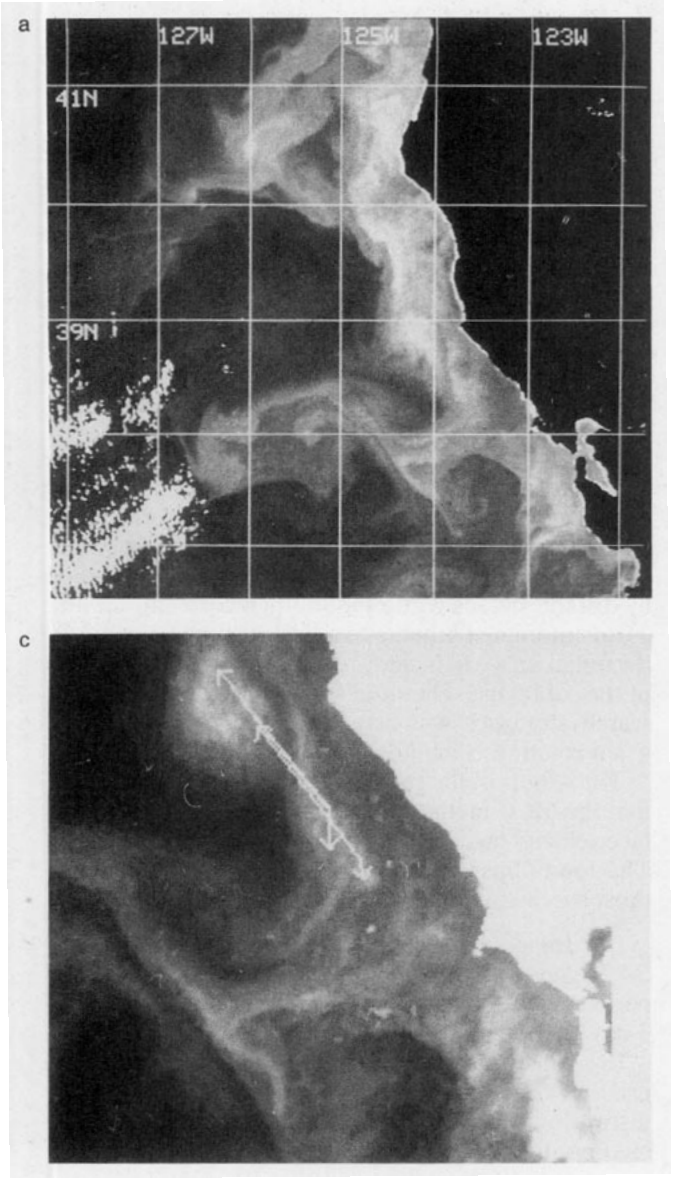

FIG. 8. (a) The CZCS image from 7 July 1981; lighter shades indicate higher pigment concentrations; (b) Contours of correlations for point A from Fig. 7b—the dark circle represents the center of the search window in the second image; (c) An expanded view of the CZCS field from 7 July 1981 (Fig. 7b) showing both the incorrect and correct displacements for points A and B in Fig. 7b.

might be based on the values of the maximum correlations associated with each vector. This would be an improvement over assigning a single value to the uncertainties of all vectors.

Another application of the MCC velocity fields is to include them in an extension of Kelly's (1989) inversion of the heat advection equation. Using a sequence of AVHRR images (identical to the sequence required in the MCC calculation), Kelly finds the velocity field that minimizes the misfit in the heat equation, subject to other constraints on divergence, vorticity, and kinetic energy. Additional constraints to minimize the difference between the final velocity field and a specified velocity field can be added, weighting the specified velocities according to their uncertainties. Use of the MCC velocities, weighted according to their maximum correlations, may provide an improvement in the along-isotherm component of the flow, which the inverse method has more difficulty in finding. Work is underway to evaluate this possibility.

5. Conclusions

Tests with both synthetic and real images suggest that the best results are found by using the vector consistency check and averaging several velocity fields obtained from images with separations of 6–12 hours. The lower limit on the rms errors in the California Current System is approximately 0.10–0.15 m s^{-1}, caused by rotation and distortion of the features by the large-scale currents, even when other nonadvective effects are minimized. Errors in magnitude and direction contribute equally in comparisons of field data and real images with separations of 12 h and more. Tests with the synthetic images suggest that errors can be reduced by using the shortest possible time separations (6 h), a conclusion in agreement with Emery et al. (1986).

The statistics of the real AVHRR and CZCS images, for this particular set of images, indicate that CZCS images separated by 24 h produce MCC velocity fields with rms errors as low as the AVHRR images separated by 12 h. The patterns in the pigment concentrations in the CZCS images used here exhibit stronger gradients which seem to persist longer than the corresponding SST fields in the AVHRR images. Although these tests furnish evidence supporting the argument that the MCC method can be applied to CZCS images with as much success as AVHRR imagery (Garcia and Robinson 1989), the method was applied to other CZCS imagery without strong fronts with less success. The key appears to be the strength of the features in the image. Even though the rms errors are similar to those from the AVHRR images, use of the CZCS images produce fewer significant vectors and a much sparser velocity field than that produced by an average of several AVHRR fields, which gives the most successful result.

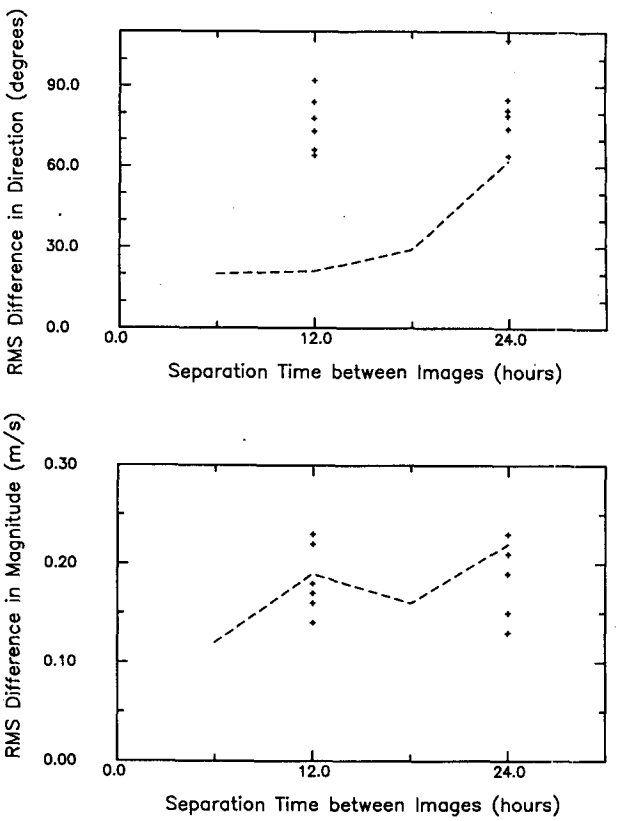

FIG. 9. Rms difference in (a) direction and (b) magnitude as a function of the time separation between images. Comparisons of model velocities to MCC velocities derived from the synthetic images is shown by the dashed line. Comparisons of the MCC velocities from each image pair to both ADCP and geostrophic velocities are shown by the crosses.

The results suggest that improvements that might be made in the MCC method include: 1) the inclusion of rotation in the search strategy; 2) improved search strategies that are more efficient and less easily fooled by distant regions with random high correlations; and 3) an automated scheme to adjust starting locations in the initial image to include regions with strong gradients in the subimage. The need for efficient and intelligent search strategies will become even more important when rotation is included in the search.

The results of the tests performed in this paper show that the MCC method successfully determines the surface velocity field in some instances and fails in others. The conditions under which the method is likely to be most successful are:

(1) Images have strong features.

(2) Several (3–5) image pairs, each separated by periods of 12 h or less, are available from a short (1–3 day) period.

(3) The resultant fields are coherent enough to allow use of a consistency check to eliminate outliers, after discarding those with correlation coefficients considered no different than random correlations.

(4) The resultant fields are then averaged.

In addition, better results are found when images come from periods when the wind has blown persistently for several days, reducing the effects of spatially varying surface heating and mixing. Even under these circumstances, absolute values of the velocity field will contain rms errors of 0.10–0.25 m s^{-1}. To put this in perspective, however, it is noted that rms differences between the ADCP and geostrophic velocities derived from data taken on the same cruise can be as large as 0.25 m s^{-1}.

These conclusions have policy implications for facilities which routinely capture and archive high resolution AVHRR data. Since the satellite-derived velocities are best for separations of 12 h and less, these operational centers should attempt to collect pairs of images with short time separations, rather than a single image on each day (a common policy). This will preserve as much of the information about surface motion as possible in the archived satellite data.

Acknowledgments. The authors benefitted from discussions with Bill Emery, Leonard Walstad, Jane Huyer, and Mike Kosro. Additional appreciation is extended to an anonymous reviewer for helpful comments. The model velocity fields were supplied by Leonard Walstad, the hydrographic data were supplied by Jane Huyer, the ADCP data were supplied by Mike Kosro, and the AVHRR and CZCS data were supplied by Mark Abbot. Support for this research came in part from NASA Grant NAGW-1251 and ONR Grant N-00014-87-K-0009.

REFERENCES

Bendat, J. S., and A. G. Piersol, 1986: *Random Data, Analysis and Measurement Procedures,* Wiley and Sons, 566 pp.

Collins, M. J., and W. J. Emery, 1988: A computational method for estimating sea ice motion in sequential Seasat synthetic aperture radar imagery by matched filtering. *J. Geophys. Res.*, **93,** 9241–9251.

Denman, K. L., and M. R. Abbott, 1986: Time evolution of surface chlorophyll patterns from cross-spectrum analysis of satellite color images. *J. Geophys. Res.*, **93,** 6789–6798.

Emery, W. J., A. C. Thomas, M. J. Collins, W. R. Crawford and D. L. Mackas, 1986: An objective method for computing advective surface velocities from sequential infrared satellite images. *J. Geophys. Res.*, **91,** 12 865–12 878.

Garcia, C. A. E., and I. S. Robinson, 1989: Sea surface velocities in shallow seas extracted from sequential Coastal Zone Color Scanner Satellite Data. *J. Geophys. Res.*, **94,** 12 681–12 691.

Kamachi, M., 1989: Advective surface velocities derived from sequential images for rotational flow field: limitations and applications of maximum cross-correlation method with rotational registration. *J. Geophys. Res.*, **94,** 18 227–18 233.

Kelly, K. A., 1989: An inverse model for near-surface velocity from infrared images. *J. Phys. Oceanogr.*, **19,** 1845–1864.

Kundu, P. K., 1976: Ekman veering observed near the ocean bottom, *J. Phys. Oceanogr.*, **6,** 238–242.

Leese, J. A., C. S. Novak and B. B. Clarke, 1971: An automated technique for obtaining cloud motion from geosynchronous satellite data using cross correlation. *J. Appl. Meteor.*, **10,** 110–132.

Mesinger, F., and A. Arakawa, 1976: *Numerical Methods Used in Atmospheric Models, Vol. 1.* Garp (Global Atmospheric Research Programme) Publications Series No. 17, 66 pp.

Olivera, M., W. E. Gilbert, J. Fleishbein, A. Huyer and R. Schramm, 1982: Hydrographic data from the first Coastal Ocean Dynamics experiment: R/V Wecoma, Leg 7, CODE Tech. Rep. 7, Data Rep. 95, Ref. 82-8, School of Oceanography, Oregon State Univ., Corvallis, 163 pp.

Press, W. H., B. P. Flannery, S. A. Teukolsky and W. T. Vetterling, 1986: *Numerical Recipes.* Cambridge University Press, 818 pp.

Robinson, A. R., and L. J. Walstad, 1987: The Harvard open ocean model: calibration and applications to dynamical process, forecasting, and data assimilation studies. *Appl. Num. Math.*, **3,** 89–131.

Svejkovsky, S., 1988: Sea surface flow estimation from Advanced Very High Resolution Radiometer and Coastal Zone Color Scanner Satellite Imagery: a verification study, *J. Geophys. Res.*, **93,** 6735–6743.

Tokmakian, R., 1989: Sea surface velocity determination using satellite imagery: validation and an application. M.S. thesis, College of Oceanography, Oregon State University, Corvallis, 105 pp.

Wahl, D. D., and J. J. Simpson, 1990: Physical processes affecting the objective determination of near-surface velocity from satellite data. *J. Geophys. Res.*, **95,** 13 511–13 528.

Vesecky, J. F., R. Samadani, J. M. Daida, M. P. Smith and R. N. Bracewell, 1987. Observing rotation and deformation of sea ice with synthetic aperture radar. *Proc. of the International Geoscience and Remote Sensing, Sensing Symposium,* IGARSS, Ann Arbor, 1137–1145.